Eur. Phys. J. Plus (2017) **132**: 345
DOI 10.1140/epjp/i2017-11609-3

THE EUROPEAN PHYSICAL JOURNAL PLUS

Regular Article

Bohr Hamiltonian for $\gamma = 0°$ with Davidson potential

Ibrahim Yigitoglu[a] and Melek Gokbulut[b]

Department of Physics, Faculty of Arts and Sciences, Gaziosmanpasa University, 60250, Tokat, Turkey

Received: 5 April 2017 / Revised: 20 May 2017
Published online: 10 August 2017 –

Abstract. A γ-rigid solution of the Bohr Hamiltonian is derived for $\gamma = 0°$ utilizing the Davidson potential in the β variable. This solution is going to be called $X(3)$-D. The energy eigenvalues and wave functions are obtained by using an analytic method which has been developed by Nikiforov and Uvarov. $B(E2)$ transition rates are calculated. A variational procedure is applied to energy ratios to determine whether or not the $X(3)$ model is located at the critical point between spherical and deformed nuclei. The agreement with the experiment is achieved.

1 Introduction

The studies describing analytically the critical point at the shape-phase transitions between different dynamical symmetries and enlightening structural properties in atomic nuclei with experimental evidence have started with the introduction of two new critical point symmetries, called $E(5)$ [1] (between $U(5)$ vibrational and $O(6)$ γ-unstable nuclei) and $X(5)$ [2] (between $U(5)$ vibrational and $SU(3)$ axially deformed nuclei). The $E(5)$ symmetry is a γ-independent exact solution of the Bohr Hamiltonian [3], while the $X(5)$ symmetry is an approximate solution for $\gamma \approx 0°$.

The method is based on constructing the Bohr Hamiltonian, choosing different types of potentials, such as Morse [4], Kratzer [5–7], Coulomb [5,6], Davidson [5], Eckart [8], Manning-Rosen [9], Killingbeck [10], and solving the eigenfunction-eigenvalue problem in search for the quadropole collective dynamics of nuclei. The geometric potentials admitting analytical solutions for the Schrödinger equation belong to two groups. The potentials in the first group depend on both β and γ and can be written in the form $V(\beta,\gamma) = V(\beta) + V(\gamma)$, where the separation of variables can be done approximately, while the potentials in the second group can be written in the form $V(\beta,\gamma) = V(\beta) + V(\gamma)/\beta^2$, where the separation of variables is done exactly [11].

Microscopic studies [12–15] indicate that the potential at the shape-phase transition point between two dynamical symmetries in atomic nuclei should be flat. Therefore an infinite square-well potential with respect to the β variable is used in the $E(5)$ and $X(5)$ symmetries.

The sequence of potentials studied in [16,17] give the opportunity to approach the $E(5)$ and $X(5)$ symmetries starting from $U(5)$. Davidson-type potentials [18], having a minimum at $\beta \neq 0$, are good candidates for approaching the $E(5)$ and $X(5)$ symmetries starting, respectively, from the $O(6)$ and $SU(3)$ limiting structures. This gives rise to exact solutions which cover all the way from $U(5)$ to $O(6)$ and from $U(5)$ to $SU(3)$. Moreover, using a variational procedure with Davidson potential the physical quantities at the critical point can be obtained [19].

The starting idea behind this study is to obtain a γ-rigid version of the $X(5)$ model constructed by assuming the nucleus to be γ-rigid, as in the Davydov and Chaban approach [20], and by fixing $\gamma = 0°$, corresponding to the axially symmetric rotor case. The model obtained in this way is called $X(3)$ [21]. Recently new studies [22–28] have been performed in this γ-rigid regime.

In the present study, a version of the $X(3)$ model is introduced by using the Davidson potential [18] in the β-part of the Schrödinger equation. This solution is going to be called the $X(3)$-D. The energy eigenvalues and wave functions are obtained by using an analytical method which has been developed by Nikiforov and Uvarov [29]. $B(E2)$ transitions rates are calculated. A variational procedure is applied for recovering the ground-state band energies of the $X(3)$ model predictions, in order to determine whether or not the $X(3)$ model is located at the critical point.

[a] e-mail: ibrahim.yigitoglu@gop.edu.tr (corresponding author)
[b] e-mail: melek.kgb@gmail.com

2 The X(3)-D solution

The original Bohr Hamiltonian lives in a five-dimensional space,

$$H = -\frac{\hbar^2}{2B}\left[\frac{1}{\beta^4}\frac{\partial}{\partial\beta}\beta^4\frac{\partial}{\partial\beta} + \frac{1}{\beta^2}\frac{1}{\sin 3\gamma}\frac{\partial}{\partial\gamma}\sin 3\gamma\frac{\partial}{\partial\gamma} - \frac{1}{4\beta^2}\sum_{\kappa}\frac{Q_\kappa^2}{\sin^2\left(\gamma - \frac{2\pi}{3}\kappa\right)}\right] + V(\beta,\gamma), \tag{1}$$

where B is the mass parameter, β and γ are the collective coordinates and $Q_\kappa(\kappa = 1,2,3)$ are the components of angular momentum in the intrinsic frame.

Considering the axially symmetric prolate case for $\gamma = 0^\circ$ [20], it is clearly seen that the motion is characterized by three collective variables (β,θ,ϕ) and the Bohr Hamiltonian takes the form

$$H = -\frac{\hbar^2}{2B}\left[\frac{1}{\beta^2}\frac{\partial}{\partial\beta}\beta^2\frac{\partial}{\partial\beta} + \frac{1}{3\beta^2}\frac{1}{\sin\theta}\frac{\partial}{\partial\theta}\sin\theta\frac{\partial}{\partial\theta} + \frac{1}{3\beta^2}\frac{1}{\sin^2\theta}\frac{\partial^2}{\partial\phi^2}\right] + V(\beta). \tag{2}$$

The wave function is

$$\psi(\beta,\theta,\phi) = F(\beta)Y_{LM}(\theta,\phi), \tag{3}$$

where $Y_{LM}(\theta,\phi)$ are the spherical harmonics.

The Schrödinger equation can be separated into β and angular parts.

$$\left[\frac{1}{\beta^2}\frac{\mathrm{d}}{\mathrm{d}\beta}\beta^2\frac{\mathrm{d}}{\mathrm{d}\beta} + \left(\varepsilon - u(\beta) - \frac{L(L+1)}{3\beta^2}\right)\right]F(\beta) = 0, \tag{4}$$

$$-\left[\frac{1}{\sin\theta}\frac{\partial}{\partial\theta}\sin\theta\frac{\partial}{\partial\theta} + \frac{1}{\sin^2\theta}\frac{\partial^2}{\partial\phi^2}\right]Y_{LM}(\theta,\phi) = L(L+1)Y_{LM}(\theta,\phi). \tag{5}$$

Here L is the angular momentum quantum number and reduced energies $\varepsilon = 2BE/\hbar^2$ and reduced potentials $u = 2BV/\hbar^2$ have been used.

In the $X(3)$ model, the β part is solved by taking an infinite square well potential, as it is done in the $X(5)$ model. In the present work, the β part is solved for the Davidson potential. Inserting the Davidson potential [18],

$$u(\beta) = \beta^2 + \frac{\beta_o^4}{\beta^2}, \tag{6}$$

into eq. (4), the "radial" equation can be rewritten as

$$\frac{\mathrm{d}^2F(\beta)}{\mathrm{d}\beta^2} + \frac{2}{\beta}\frac{\mathrm{d}F(\beta)}{\mathrm{d}\beta} + \left[\varepsilon - \frac{L(L+1)}{3\beta^2} - \beta^2 - \frac{\beta_o^4}{\beta^2}\right]F(\beta) = 0. \tag{7}$$

Plugging the Davidson potential into eq. (7) gives rise to an exact solution [30,31]. In order to solve eq. (7), it is transformed into the Nikiforov-Uvarov (NU) equation form. The NU equation reads

$$\psi''(z) + \frac{\tilde\tau(z)}{\sigma(z)}\psi'(z) + \frac{\tilde\sigma(z)}{\sigma^2(z)}\psi(z) = 0, \tag{8}$$

where $\sigma(z)$ and $\tilde\sigma(z)$ are at most second degree polynomials, while $\tilde\tau(z)$ is a first degree polynomial. For this purpose the $\beta^2 = z$ change of variable is applied to eq. (7) and

$$\frac{\mathrm{d}^2F(z)}{\mathrm{d}z^2} + \frac{3}{2z}\frac{\mathrm{d}F(z)}{\mathrm{d}z} + \frac{1}{4z^2}\left[-z^2 + \varepsilon z - \alpha\right]F(z) = 0 \tag{9}$$

is obtained. We compared eqs. (8) and (9) and then we determined the parametric polynomials as follows:

$$\tilde\tau(z) = 3, \qquad \sigma(z) = 2z, \qquad \tilde\sigma(z) = -z^2 + \varepsilon z - \alpha, \tag{10}$$

where $\alpha = \beta_o^4 + \frac{L(L+1)}{3}$. The functions and the parameters required for this method are defined as follows:

$$\begin{aligned}
\pi(z) &= \sigma'(z) - \tilde\tau(z)/2 \pm \left[\left(\sigma'(z) - \tilde\tau(z)/2\right)^2 - \tilde\sigma(z) + k\sigma(z)\right]^{1/2},\\
\tau(z) &= \tilde\tau(z) + 2\pi(z),\\
\lambda &= k + \pi'(z),\\
\lambda_n &= -n\tau' - \frac{n(n-1)}{2}\sigma'' \qquad n = 0,1,2,\ldots
\end{aligned} \tag{11}$$

For $\lambda = \lambda_n$, one obtains the energy eigenvalues. By using the parametric polynomials, we get the equalities

$$\begin{aligned} k_- &= \varepsilon/2 - \sqrt{\alpha + 1/4}, \\ \pi(z) &= -1/2 - \left[z - \sqrt{\alpha + 1/4}\right], \\ \lambda &= \varepsilon/2 - \sqrt{\alpha + 1/4} - 1, \\ \lambda_n &= 2n. \end{aligned} \tag{12}$$

Finally, we obtained the energy equation,

$$E_{n,L} = 2n + 1 + \sqrt{\beta_o^4 + \frac{L(L+1)}{3} + \frac{1}{4}}\,, \tag{13}$$

where n is the usual oscillator quantum number, L is the angular momentum quantum number, and β_o corresponds to the position of the minimum of the potential. In eq. (13), $n = 0$ corresponds to the ground-state band (gsb).

The eigenfunction is written in the form of $F(z) \to \psi(z) = \varphi(z) y_n(z)$. Following the NU method,

$$\begin{aligned} \frac{\varphi'(z)}{\varphi(z)} &= \frac{\pi(z)}{\sigma(z)}\,, \\ y_n &= \frac{B_n}{\rho(z)} \frac{\mathrm{d}^n}{\mathrm{d}z^n} \left[\sigma^n(z)\rho(z)\right], \\ \left[\sigma(z)\rho(z)\right]' &= \tau(z)\rho(z). \end{aligned} \tag{14}$$

We have calculated $\varphi(z)$ and $y_n(z)$ and the eigenfunction is written with respect to the β variable as

$$F(\beta) = C_N \beta^a e^{-\beta^2/2} L_n^{a+1/2}(\beta^2), \tag{15}$$

where C_N is the normalization constant, $a = -\frac{1}{2} + \sqrt{\beta_o^4 + \frac{L(L+1)}{3} + \frac{1}{4}}$, and L_n are the Laguerre polynomials.

The C_N normalization constant is obtained from the condition $\int_0^\infty F^2(\beta)\beta^2 \mathrm{d}\beta = 1$. Then the final expression for the eigenfunction is

$$F(\beta) = \left[\frac{2}{\Gamma\left(a + \frac{3}{2}\right)\binom{n + a + 1/2}{n}}\right]^{1/2} \beta^a e^{-\beta^2/2} L_n^{a+1/2}(\beta^2). \tag{16}$$

The energy ratios $R_{n,L}$ play an important role in investigating the structural evolution. They are defined as

$$R_{n,L} = \frac{E_{0,L} - E_{0,0}}{E_{0,2} - E_{0,0}}\,. \tag{17}$$

3 B(E2) transition rates

The general form of the quadrupole operator is

$$T_\mu^{(E2)} = t\beta \left[D_{\mu,0}^{2^*}(\Omega)\cos\gamma + \frac{1}{\sqrt{2}}\left[D_{\mu,2}^{2^*}(\Omega) + D_{\mu,-2}^{2^*}(\Omega)\sin\gamma\right]\right], \tag{18}$$

where t denotes a scalar factor and Ω the Euler angles. The quadrupole operator [21] for $\gamma = 0$ is

$$T_\mu^{(E2)}(\beta) = t\beta\sqrt{\frac{4\pi}{5}} Y_{2\mu}(\theta, \phi). \tag{19}$$

Then the $B(E2)$ rates are

$$B(E2; nL \to n'L') = t^2 \left(C_{L0,20}^{L'0}\right)^2 I_{nL;n'L'}^2, \tag{20}$$

where $C_{L0,20}^{L'0}$ are Clebsch-Gordan coeffients and the integrals are

$$I_{nL \to n'L'} = \int_0^\infty \beta F_{nL}(\beta) F_{n'L'}(\beta) \beta^2 \mathrm{d}\beta. \tag{21}$$

Table 1. Energy levels of the $X(3)$-D model corresponding to different β_o values. Ground-state band, β_1 and β_2 band energies are normalized to the $2_{1,0}$ band lowest excited state. The $X(3)$ model predictions and variational procedure for energy levels are placed for comparison reason. See sect. 4 for further discussion.

gsb	β_o	0	1	1.5	2	∞	$\beta_{o,m}$	var	$X(3)$
	$L_{s,n}$								
	$0_{1,0}$	0.00	0.00	0.00	0.00	0.00			0.00
	$2_{1,0}$	1.00	1.00	1.00	1.00	1.00			1.00
	$4_{1,0}$	2.13	2.48	2.90	3.14	3.33	1.10	2.57	2.44
	$6_{1,0}$	3.27	4.07	5.23	6.10	7.00	1.24	4.62	4.23
	$8_{1,0}$	4.42	5.71	7.79	9.60	12.00	1.35	7.13	6.35
	$10_{1,0}$	5.58	7.36	10.45	13.46	18.33	1.44	10.05	8.78
	$12_{1,0}$	6.73	9.02	13.19	17.56	26.00	1.53	13.47	11.52
	$14_{1,0}$	7.88	10.69	15.96	21.82	35.00	1.61	17.30	14.57
	$16_{1,0}$	9.04	12.37	18.76	26.19	45.33	1.68	21.59	17.91
	$18_{1,0}$	10.19	14.05	21.58	30.65	57.00	1.76	26.30	21.56
β_1	β_o	0	1	1.5	2		$\beta_{o,m}$	var	$X(3)$
	$L_{s,n}$								
	$0_{2,1}$	2.00	2.92	5.01	8.30				2.87
	$2_{2,1}$	3.00	3.92	6.01	9.30				4.83
	$4_{2,1}$	4.13	5.40	7.90	11.44				7.37
	$6_{2,1}$	5.27	6.99	10.24	14.40				10.29
	$8_{2,1}$	6.42	8.63	12.80	17.91				13.57
	$10_{2,1}$	7.58	10.28	15.46	21.77				17.18
	$12_{2,1}$	8.73	11.94	18.20	25.87				21.14
β_2	β_o	0	1	1.5	2		$\beta_{o,m}$	var	$X(3)$
	$L_{s,n}$								
	$0_{3,2}$	4.00	5.84	10.02	16.61				7.65
	$2_{3,2}$	5.00	6.84	11.02	17.61				10.56
	$4_{3,2}$	6.13	8.32	12.91	19.75				14.19
	$6_{3,2}$	7.27	9.91	15.25	22.70				18.22
	$8_{3,2}$	8.42	11.55	17.81	26.21				22.62

4 Numerical results

The lowest bands for the $X(3)$-D solution can be seen for various values of the parameter β_o in table 1. The ground-state band is characterized by $(n = 0, s = 1)$. The β_1 band is characterized by $(n = 1, s = 2)$, while the β_2 band is characterized by $(n = 2, s = 3)$. The $X(3)$ and $X(3)$-D spectra can be compared through the correspondence $n = s-1$. The energy levels are represented by $L_{s,n}$. The energy levels of all bands are normalized to the energy of the lowest excited $2_{1,0}$ level. In addition, the energy levels resulting from the variational procedure are reported (labelled by "var"), along with the parameter values $\beta_{o,m}$ at which they are obtained.

The ground-state band energies are shown in fig. 1. It is clear that the energy levels for $\beta_o = 0$ approach to the $U(5)$ vibrational limit, while $\beta_o \to \infty$ corresponds to the $SU(3)$ rotational limit. The spectra obtained for $\beta_o = 1.5$ and $\beta_o = 2$ are similar to the $X(3)$ and $X(5)$ model predictions, respectively. It can be seen that with increasing β_o values the way from $U(5)$ to $SU(3)$ is spanned.

The variational procedure as it is introduced in ref. [19] can be used as a tool for determining the behavior of the physical quantities at the point of shape-phase transitions in nuclei. It differs from the standard Ritz method of quantum mechanics [32]. In the Ritz approach the main idea is minimizing the energy, while in the present case it is achieved by maximizing the rate of change of the physical quantity. It is applied by determining the parameter value that corresponds to the maximum increase of a physical quantity at the critical point, while using a potential with one parameter spanning the region between the two limiting structures.

The $R_{n,L}$ ratios are structural signatures that serve for searching the shape-phase transition and the critical point between two limiting symmetries. The determination of the β_o values at which the rate of change of $R_{n,L}$ becomes maximum is crucial, since the structural evolution at the critical point changes rapidly. Therefore we applied the variational procedure and compared the obtained results to the $X(3)$ model predictions to determine whether or not

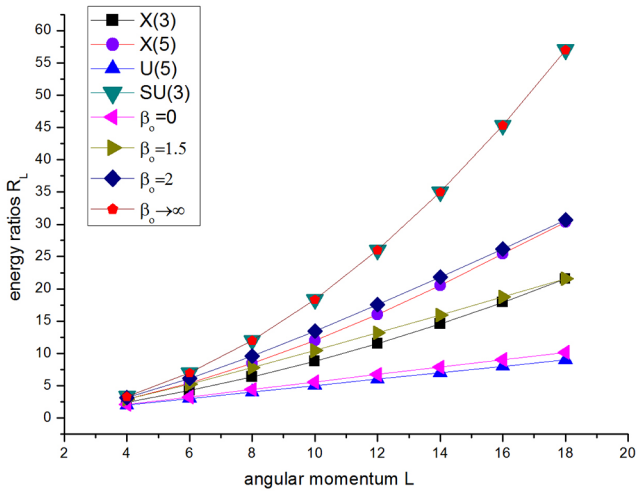

Fig. 1. The energy ratios R_L *vs.* angular momentum L are shown for different β_o values and are compared with the $U(5)$, $SU(3)$, $X(5)$ and $X(3)$ predictions. All energy levels are normalized to the lowest excited state.

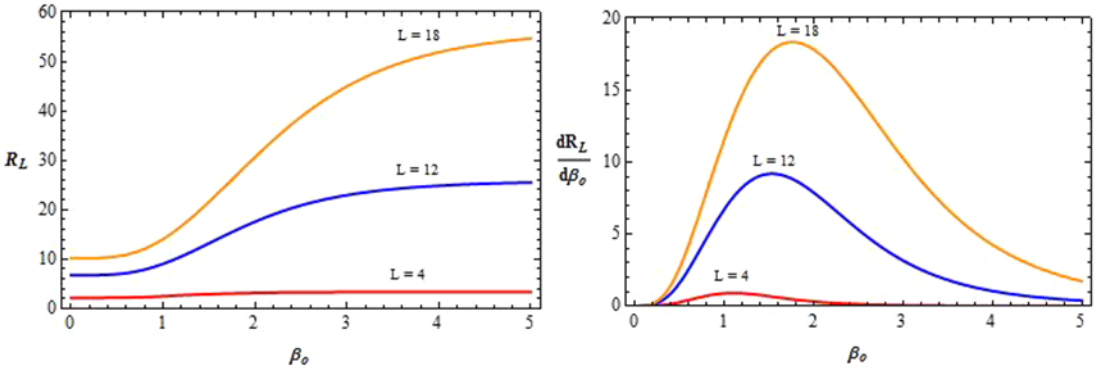

Fig. 2. The R_L ratios for $L = 4, 12, 18$ and their derivatives $\mathrm{d}R_L/\mathrm{d}\beta_o$ *vs.* the β_o parameter values obtained using the Davidson potential in the $X(3)$-D model.

the $X(3)$ model is located at the critical point between the spherical vibrator $U(5)$ and the axially symmetric prolate rotor $SU(3)$.

The $R_{n,L}$ curves exhibited in fig. 2 show the evolution of nuclear structure from the $U(5)$ symmetry on the left hand side to the $SU(3)$ symmetry on the right hand side. The $R_{n,L}$ ratios increase with the β_o values. The curve has the steepest increase at the point $\beta_{o,m}$, where the first derivative acquires its maximum value, while the second derivative $\mathrm{d}^2R_{n,L}/\mathrm{d}\beta_o^2$ vanishes at this point.

Numerical results for $\beta_{o,m}$ and the corresponding $R_{n,L}$ ratios (labelled as var) obtained through the variational procedure are shown in table 1. We see that the output of the variational procedure (the "var" column) is quite similar to the $X(3)$ results, although the agreement is not as strong as in the studies where the same comparison is made between the variational procedure and the $E(5)$ and $X(5)$ model predictions [19]. This discrepancy may be attributed to the γ-rigid nature of the $X(3)$ model, where γ is a parameter and not a variable.

The ground-state band energies obtained for different β_o values are compared with the existing experimental data of the $^{172\text{-}180}$Os, ^{156}Dy, ^{154}Gd isotopes in fig. 3(a) and ^{104}Ru, ^{148}Nd, ^{186}Pt, ^{196}Pt, ^{120}Xe, ^{126}Xe isotopes in fig. 3(b). The $X(5)$ and $X(3)$ model predictions are also shown in the figures for comparison.

The ^{172}Os ground-state band (gsb) energies are in good agreement with $X(3)$-D (with $\beta_o = 1.310$) and $X(3)$ model predictions up to $L = 12$. The $X(3)$-D model predictions with increasing β_o values move to the $X(5)$ model side and become consistent with the $X(5)$ model and the ^{176}Os data for $\beta_o = 1.863$ up to $L = 14$. The $^{178\text{-}180}$Os data are also lying close to $X(5)$, described by $X(3)$-D with $\beta_o = 1.910$ and 2.0, respectively.

The well-known $X(5)$ model candidates ^{154}Gd and ^{156}Dy are in good agreement with the $X(3)$-D model for $\beta_o = 1.980$ and $\beta_o = 1.905$, respectively, in fig. 3(a). This is a piece of evidence on how the $X(3)$-D solution spans the path from the $U(5)$ symmetry to the $SU(3)$ symmetry, as it is also seen in fig. 2.

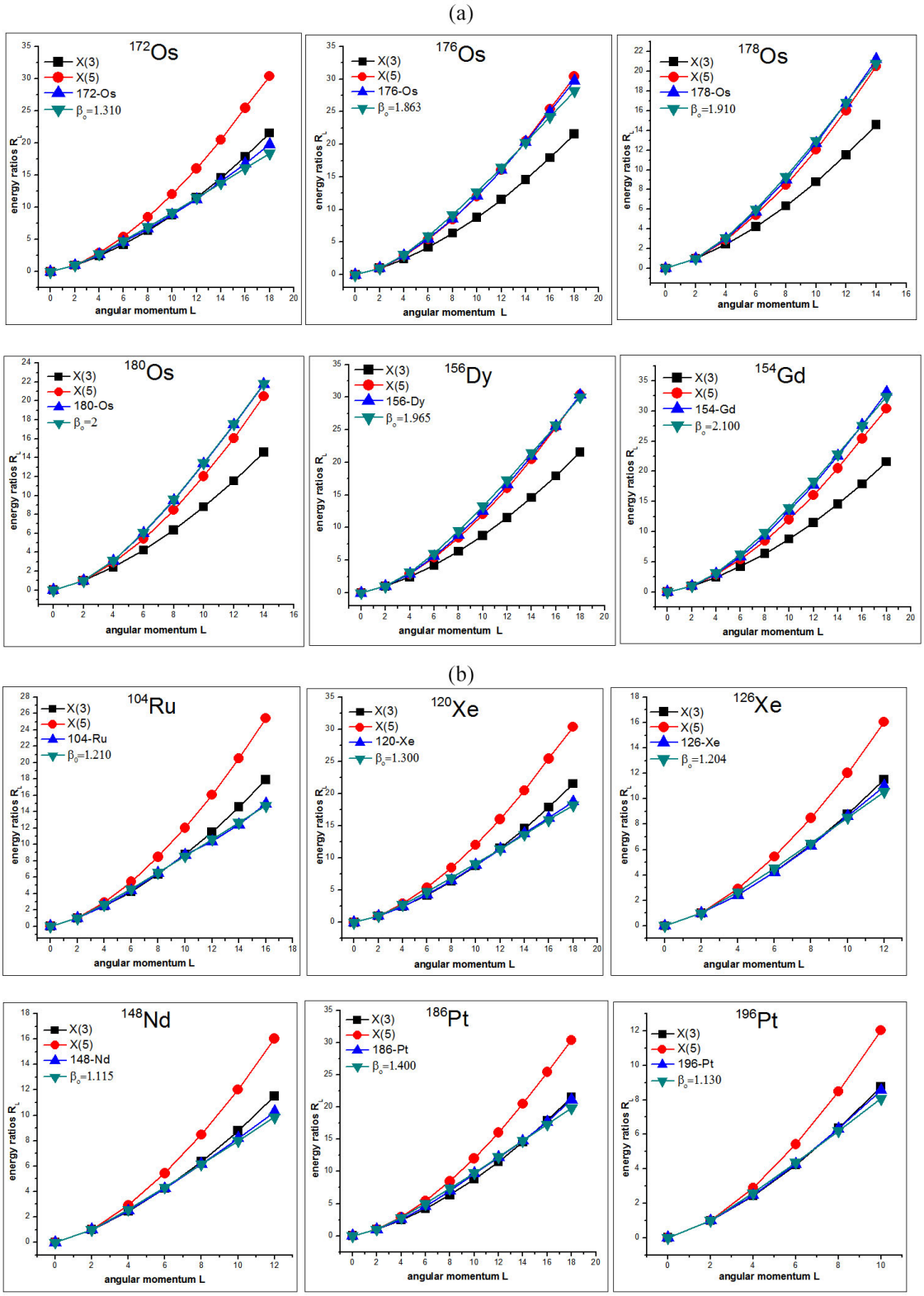

Fig. 3. (a) The $X(3)$-D model ground-state band energy predictions obtained for different β_o values are compared with the data for $^{172\text{-}180}$Os, ^{154}Gd and ^{156}Dy. The $X(5)$ and $X(3)$ model predictions are also shown for comparison. (b) The $X(3)$-D model ground-state band energy predictions obtained for different β_o values are compared with the data of ^{104}Ru, ^{120}Xe, ^{126}Xe, ^{148}Nd, ^{186}Pt and ^{196}Pt. The $X(5)$ and $X(3)$ model predictions are also shown for comparison.

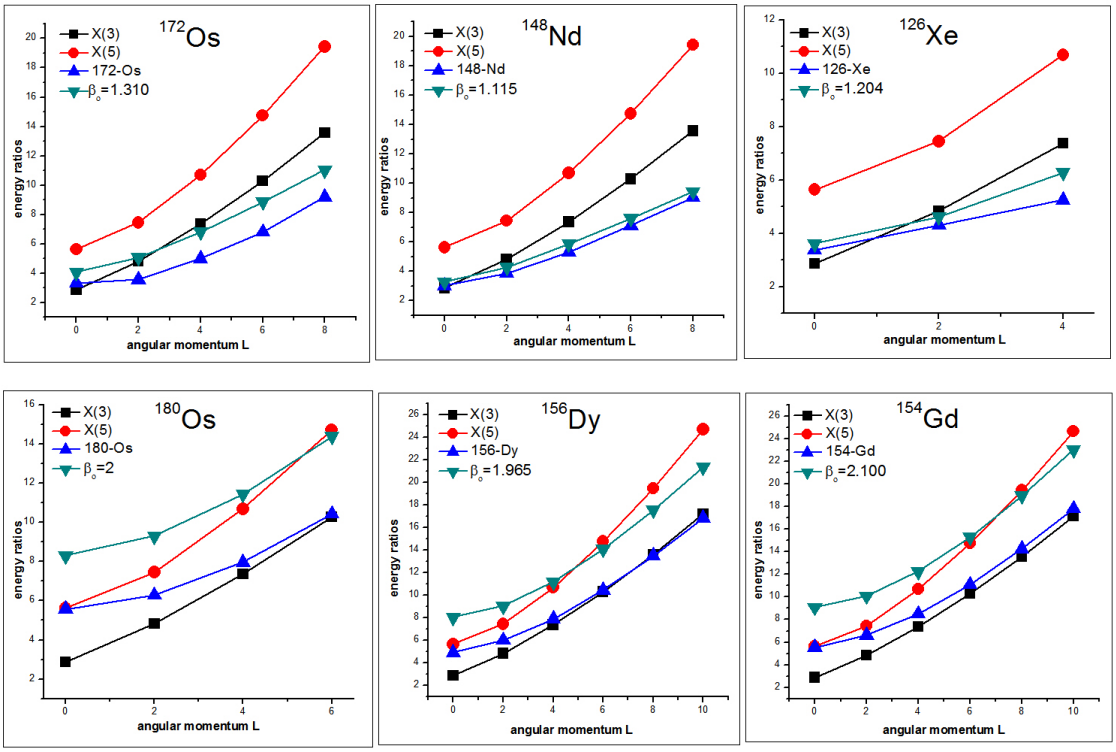

Fig. 4. The β_1 band energies obtained for different β_o values are compared with the existing experimental data of ^{172}Os, ^{180}Os, ^{148}Nd, ^{126}Xe, ^{156}Dy and ^{154}Gd isotopes. The $X(5)$ and $X(3)$ model predictions are also shown for comparison.

The $X(3)$ model prediction for gsb is in good agreement with ^{104}Ru up to $L = 10$ and with ^{148}Nd up to $L = 8$ in fig. 3(b). Both ^{104}Ru and ^{148}Nd isotopes show better agreement up to higher L with $X(3)$-D (with $\beta_o = 1.210$ and 1.115, respectively).

The same behavior can be observed in fig. 3(b) for the Xe isotopes. The $X(3)$ model gsb is in good agreement with ^{120}Xe up to $L = 12$ and with ^{126}Xe up to $L = 10$, while a better agreement up to higher L can be seen with $X(3)$-D (with $\beta_o = 1.300$ and 1.204, respectively).

A similar behavior can be observed for the Pt isotopes. ^{186}Pt and ^{196}Pt gsb data are well produced with $X(3)$-D (with $\beta_o = 1.400$ and 1.130, respectively).

The β_1 band energies obtained for different β_o values are compared with the existing experimental data of ^{172}Os, ^{180}Os, ^{148}Nd, ^{126}Xe, ^{156}Dy and ^{154}Gd isotopes in fig. 4. The $X(5)$ and $X(3)$ model predictions are also shown for comparison.

It can be seen from fig. 4 that ^{148}Nd shows the best agreement in the β_1 bands with $X(3)$-D model predictions. There is also consistency with the β_1 bands of ^{172}Os and ^{126}Xe isotopes and the $X(3)$-D model predictions. ^{180}Os, ^{156}Dy and ^{154}Gd isotopes β_1 bands data shown in fig. 4 are inconsistent with $X(3)$-D β_1 band predictions which lay high in energy.

The ground-state band energies and the β_1 band head of these three isotopes are in agreement with $X(5)$ model predictions while the β_1 bands of these three isotopes from $L = 4$ upwards agree with the $X(3)$ model predictions. This behavior could be explained by the γ degree of freedom that could affect the β band heads.

The ground-state and β_1 bands energy ratios ($R_{n,L}$) obtained in eq. (17) for $X(3)$-D solution are given in table 2 with $X(3)$-Sextic [25] predictions and the available experimental data for $^{172\text{-}180}$Os, ^{154}Gd, ^{156}Dy, ^{104}Ru, ^{120}Xe, ^{126}Xe, ^{148}Nd, ^{186}Pt and ^{196}Pt nuclei. It can be seen in table 2 that ^{172}Os, ^{154}Gd, ^{156}Dy, ^{186}Pt ground-state bands (gsb) show good agreement with the $X(3)$-D while the β_1 bands are consistent with the $X(3)$-Sextic solution.

^{148}Nd isotope data are well reproduced with $X(3)$-D solution even for gsb or β_1 bands than $X(3)$-Sextic. The gsb predictions in both solutions are similar for ^{126}Xe and ^{196}Pt while the β_1 bands for two isotopes are predicted better with $X(3)$-D solution. The two solutions have similar agreement with ^{104}Ru gsb and β_1 bands data. The $X(3)$-D model have a very good consistency with $^{176\text{-}180}$Os isotopes gsb bands while the β_1 bands predictions of $X(3)$-D model lay higher in energy. There is no prediction for $^{176\text{-}180}$Os isotopes were made in $X(3)$-Sextic solution in ref. [25]. Although both $X(3)$-D and $X(3)$-Sextic β_1 bands predictions show good agreement with some of nuclei in table 2, it is difficult to say which $K = 0^+$ bands are the β bands and which are due to other types of excitations [33].

Table 2. The ground-state and β_1 bands energy ratios ($R_{n,L}$) obtained in eq. (17) by $X(3)$-D solution are given with $X(3)$-S (S: Sextic potential) model predictions and the available experimental data for $^{172\text{-}180}$Os, ^{154}Gd, ^{156}Dy, ^{104}Ru, ^{120}Xe, ^{126}Xe, ^{148}Nd, ^{186}Pt and ^{196}Pt.

Nucleus	$R_{0,4}$	$R_{0,6}$	$R_{0,8}$	$R_{0,10}$	$R_{1,0}$	$R_{1,2}$	$R_{1,4}$	$R_{1,6}$
^{172}Os	2.66	4.63	6.7	8.89	3.33	3.56	5	6.81
$X(3)$-D	2.75	4.8	6.97	9.2	4.07	5.07	6.82	8.86
$X(3)$-S	2.65	4	6.1	7.63	2.77	4.06	6.07	7.62
^{176}Os	2.93	5.5	8.57	12.10	4.45	5.5	7.59	10.6
$X(3)$-D	3.09	5.91	9.18	12.72	7.28	8.29	10.38	13.20
$X(3)$-S	No data							
^{178}Os	3.02	5.76	9.03	12.72	4.92	5.8	7.74	10.56
$X(3)$-D	3.11	5.98	9.32	12.98	7.63	8.63	10.73	13.99
$X(3)$-S	No data							
^{180}Os	3.09	6.01	9.5	13.38	5.57	6.29	7.97	10.44
$X(3)$-D	3.14	6.1	9.6	13.5	8.30	9.30	11.44	14.40
$X(3)$-S	No data							
^{154}Gd	3.01	5.83	9.3	13.3	5.53	6.63	8.51	11.1
$X(3)$-D	3.17	6.62	9.88	13.96	9.1	10.1	12.26	15.31
$X(3)$-S	2.53	4.46	7.21	9.7	4.33	6.5	8.84	11.58
^{156}Dy	2.93	5.59	8.82	12.52	4.9	6.01	7.9	10.43
$X(3)$-D	3.13	6.05	9.49	13.28	8.04	9.04	11.16	14.09
$X(3)$-S	2.53	4.46	7.20	9.68	4.31	6.46	8.81	11.53
^{104}Ru	2.48	4.35	6.48	8.69		4.2	5.81	
$X(3)$-D	2.66	4.55	6.54	8.57	3.64	4.64	6.31	8.2
$X(3)$-S	2.74	4.14	6.41	8.02	2.92	4.28	6.45	8.10
^{120}Xe	2.47	4.33	6.51	8.90	2.82	3.95	5.31	
$X(3)$-D	2.75	4.8	6.97	9.20	4.07	5.07	6.82	8.80
$X(3)$-S	2.73	4.11	6.32	7.91	2.88	4.21	6.34	7.94
^{126}Xe	2.42	4.21	6.27	8.64	3.38	4.32	5.25	
$X(3)$-D	2.66	4.54	6.51	8.53	3.62	4.62	6.28	8.16
$X(3)$-S	2.72	4.09	6.29	7.86	2.86	4.18	6.3	7.89
^{148}Nd	2.49	4.24	6.15	8.19	3.04	3.88	5.32	7.12
$X(3)$-D	2.58	4.33	6.15	8.0	3.29	4.29	5.87	7.62
$X(3)$-S	2.61	3.95	5.98	7.49	2.71	3.98	5.94	7.46
^{186}Pt	2.56	4.58	7.01	9.7	2.46	4.17	6.38	8.36
$X(3)$-D	2.82	5.01	7.36	9.79	4.49	5.49	7.31	9.5
$X(3)$-S	2.68	4.18	6.53	8.3	3.04	4.56	6.8	8.64
^{196}Pt	2.47	4.29	6.33	8.56	3.19	3.83		
$X(3)$-D	2.59	4.37	6.21	8.08	3.34	4.34	5.93	7.71
$X(3)$-S	2.72	4.15	6.45	8.13	2.96	4.39	6.59	8.31

$B(E2)$ rates of $X(3)$-D model corresponding to different β_o values for the gsb, β_1 and β_2 bands are given in table 3. It is seen that $B(E2)$ rates obtained for the $X(3)$-D solution decrease with increasing β_o values. The $X(3)$ model predictions for gsb lie in between the $X(3)$-D predictions obtained for $\beta_o = 1$ and $\beta_o = 1.5$. This behavior in gsb $B(E2)$ values is not observed for the β bands.

Table 3. $B(E2; L_f \to L_i)$ rates for the $X(3)$-D model corresponding to different β_o values for the ground-state band, β_1 and β_2 bands. The $B(E2)$ rates are normalized to the $B(E2; 2_{1,0} \to 0_{1,0})$ transition rate value from the lowest excited state to the ground state. The $X(3)$ model predictions are placed for comparison reason.

β_o	0	1	1.5	2	5	$X(3)$
$L_i \to L_s$						
$2_{1,0} \to 0_{1,0}$	1.000	1.000	1.000	1.000	1.000	1.000
$4_{1,0} \to 2_{1,0}$	2.377	1.912	1.638	1.522	1.432	1.889
$6_{1,0} \to 4_{1,0}$	3.803	2.864	2.180	1.854	1.584	2.489
$8_{1,0} \to 6_{1,0}$	5.237	3.854	2.759	2.185	1.669	2.914
$10_{1,0} \to 8_{1,0}$	6.677	4.862	3.370	2.538	1.729	3.238
$12_{1,0} \to 10_{1,0}$	8.117	5.878	3.998	2.910	1.777	3.495
$14_{1,0} \to 12_{1,0}$	9.557	6.900	4.638	3.298	1.821	3.707
$16_{1,0} \to 14_{1,0}$	10.997	7.926	5.287	3.698	1.862	3.885
$18_{1,0} \to 16_{1,0}$	12.440	8.952	5.941	4.105	1.903	4.037
$2_{2,1} \to 0_{2,1}$	1.667	1.613	1.452	1.306	1.058	0.806
$4_{2,1} \to 2_{2,1}$	3.203	2.585	2.179	1.926	1.515	1.401
$6_{2,1} \to 4_{2,1}$	4.693	3.544	2.700	2.256	1.676	1.824
$8_{2,1} \to 6_{2,1}$	6.163	4.542	3.261	2.571	1.764	2.155
$10_{2,1} \to 8_{2,1}$	7.623	5.556	3.860	2.907	1.826	2.424
$12_{2,1} \to 10_{2,1}$	9.077	6.580	4.481	3.267	1.875	2.651
$14_{2,1} \to 12_{2,1}$	10.530	7.606	5.120	3.646	1.918	
$16_{2,1} \to 14_{2,1}$	11.980	8.635	5.766	4.038	1.959	
$18_{2,1} \to 16_{2,1}$	13.427	9.663	6.418	4.440	2.000	
$20_{2,1} \to 18_{2,1}$	14.877	10.695	7.075	4.850	2.041	
$22_{2,1} \to 20_{2,1}$	16.323	11.726	7.733	5.266	2.083	
$2_{3,2} \to 0_{3,2}$	2.333	2.229	1.908	1.616	1.117	0.735
$4_{3,2} \to 2_{3,2}$	4.027	3.260	2.722	2.333	1.599	1.205
$6_{3,2} \to 4_{3,2}$	5.583	4.224	3.220	2.661	1.768	1.542
$8_{3,2} \to 6_{3,2}$	7.090	5.232	3,762	2,957	1,860	1.812
$10_{3,2} \to 8_{3,2}$	8.573	6.253	4.351	3.276	1.923	
$12_{3,2} \to 10_{3,2}$	10.043	7.282	4.966	3.623	1.973	
$14_{3,2} \to 12_{3,2}$	11.503	8.313	5.599	3.992	2.016	
$16_{3,2} \to 14_{3,2}$	12.963	9.346	6.244	4.378	2.057	
$18_{3,2} \to 16_{3,2}$	14.417	10.377	6.894	4.775	2.097	
$20_{3,2} \to 18_{3,2}$	15.870	11.411	7.551	5.182	2.137	
$22_{3,2} \to 20_{3,2}$	17.320	12.446	8.211	5.594	2.178	

5 Conclusion

In this study a γ-rigid solution of the Bohr Hamiltonian is obtained by solving the β part with a Davidson potential. This solution is called $X(3)$-D. The energy eigenvalues and wave functions are obtained by using an analytic method which has been developed by Nikiforov and Uvarov. $B(E2)$ transition rates are also calculated. The $X(3)$-D model spans the path from the $U(5)$ symmetry to the $SU(3)$ symmetry involving a free parameter β_o. Applying a variational procedure we point out that it is possible to suggest the $X(3)$ model as a solution for a critical point symmetry. The $X(3)$-D solution gives us the opportunity to search the experimental data on the path from the $U(5)$ symmetry to the $SU(3)$ symmetry.

The authors acknowledge financial support by the Scientific and Technical Research Council of Turkey (TUBITAK), under the project number TBAG (112T754).

References

1. F. Iachello, Phys. Rev. Lett. **85**, 3580 (2000).
2. F. Iachello, Phys. Rev. Lett. **87**, 052502 (2001).
3. A. Bohr, Mat. Fys. Medd. K. Dan. Vidensk. Selsk. **26**, No. 14 (1952).
4. I. Boztosun, D. Bonatsos, I. Inci, Phys. Rev. C **77**, 044302 (2008).
5. L. Fortunato, S. De Baerdemacker, K. Heyde, Phys. Rev. C **74**, 014310 (2006).
6. L. Fortunato, A. Vitturi, J. Phys. G Nucl. Part. Phys. **30**, 627 (2004).
7. D. Bonatsos, P.E. Georgoudis, N. Minkov, Phys. Rev. C **88**, 034316 (2013).
8. L. Naderi, H. Hassanabadi, Eur. Phys. J. Plus **131**, 5 (2016).
9. M. Chabab, A. El Batoul, A. Lahbas, M. Oulne, Nucl. Phys. A **953**, 158 (2016).
10. H. Sobhani, H. Hassanabadi, Mod. Phys. Lett. A **31**, 1650152 (2016).
11. L. Fortunato, Eur. Phys. J. A **26**, s01 1 (2005).
12. J. Meng, W. Zhang, S.G. Zhou, H. Toki, L.S. Geng, Eur. Phys. J. A **25**, 23 (2005).
13. Z.Q. Sheng, J.Y. Guo, Mod. Phys. Lett. A **20**, 2711 (2005).
14. T. Niksic, D. Vretenar, G.A. Lalazissis, Phys. Rev. Lett. **99**, 092502 (2007).
15. Z.P. Li, T. Niksic, D. Vretenar, Phys. Rev. C **80**, 061301 (2009).
16. D. Bonatsos, D. Lenis, N. Minkov, P.P. Raychev, P.A. Terziev, Phys. Rev. C **69**, 014302 (2004).
17. D. Bonatsos, D. Lenis, N. Minkov, P.P. Raychev, P.A. Terziev, Phys. Rev. C **69**, 044316 (2004).
18. P.M. Davidson, Proc. R. Soc. London, Ser. A **135**, 459 (1932).
19. D. Bonatsos, D. Lenis, N. Minkov, D. Petrellis, P.P. Raychev, P.A. Terziev, Phys. Lett. B **584**, 40 (2004).
20. A.S. Davydov, A.A. Chaban, Nucl. Phys. **20**, 499 (1960).
21. D. Bonatsos, D. Lenis, D. Petrellis, P.A. Terziev, I. Yigitoglu, Phys. Lett. B **632**, 238 (2006).
22. M. Alimohammadi, H. Hassanabadi, Nucl. Phys. A **957**, 439 (2017).
23. M. Alimohammadi, H. Hassanabadi, S. Zare, Nucl. Phys. A **960**, 78 (2017).
24. M. Chabab, A. El Batoul, A. Lahbas, M. Oulne, Phys. Lett. B **758**, 212 (2016).
25. P. Buganu, R. Budaca, J. Phys. G: Nucl. Part. Phys. **42**, 105106 (2015).
26. R. Budaca, Phys. Lett. B **739**, 56 (2014).
27. R. Budaca, A.I. Budaca, J. Phys. G: Nucl. Part. Phys. **42**, 085103 (2015).
28. M. Chabab, A. El Batoul, A. Lahbas, M. Oulne, J. Phys. G: Nucl. Part. Phys. **43**, 125107 (2016).
29. A.F. Nikiforov, V.B. Uvarov, *Special Functions of Mathematical Physics* (Birkhaüser Basel, 1988).
30. J.P. Elliott, J.A. Evans, P. Park, Phys. Lett. B **169**, 309 (1986).
31. D.J. Rowe, C. Bahri, J. Phys. A **31**, 4947 (1998).
32. W. Greiner, *Quantum Mechanics – An Introduction* (Springer, Berlin 1989).
33. P.E. Garrett, J. Phys. G: Nucl. Part. Phys. **27**, R1 (2001).